Exploring the benefits and pitfalls of using multiples in imaging

Gordon Poole[1]* and Milad Farshad[1] demonstrate how the use of multiples in imaging may provide improved shallow illumination and potentially reduce the requirement for extensive site-survey acquisition in some areas.

Introduction

Many modern acquisition geometries using wide-tow streamer or ocean-bottom node (OBN) designs are optimised for the efficient illumination of deep targets using primary arrivals. One disadvantage of such configurations is that they often result in heavy striping when imaging the shallower section, owing to a lack of primary arrivals with small reflection angles. This may relate either to limited near-offset recordings from outer towed streamers or shots located away from the OBN receiver lines. With OBN geometries, down-going mirror migration may improve imaging of the shallow section, but the result may still be stripy and contaminated by noise, owing to the limited illumination between receiver lines. The use of free-surface multiples to enhance subsurface illumination has been discussed in the literature for many years (Berkhout and Verschuur, 1994). A free-surface multiple imaging approach that involves re-injection of recorded data as secondary sources has been shown to provide superior shallow imaging when compared to imaging using primaries alone (Mujis et al., 2005, Whitmore et al., 2010, Poole, 2021a).

Primary imaging using one-way wave-equation migration involves source-side injection and subsequent forward propagation of a source wavelet, synchronised with the backward propagation of recorded data after demultiple on the receiver-side. At depths where the forward- and backward-propagated wavefields correlate in time and space, a subsurface image is formed using a cross-correlation or deconvolution imaging condition. Multiple imaging involves the injection of recorded data as secondary sources for both the source and receiver sides. The illumination from all multiple orders occurs simultaneously when forward-propagated arrivals correlate with the subsequent multiple order on the backward-propagated wavefield.

Figure 1 compares primary imaging and multiple imaging depth slices from a towed-streamer acquisition in the Central North Sea. The acquisition utilised a dual-source configuration towing ten streamers with a 100 m separation. Figure 1a illustrates a vessel sailing into the page with a water bottom primary arrival ray-path annotated. A water velocity v_w = 1500 m.s^{-1}, with a water bottom velocity v_{wb} = 1800 m.s^{-1}, gives a critical angle of θ_c = 56° (Snell's law: $\theta_c = sin^{-1}(v_w/v_{wb})$). The water bottom depth in this area was 92 m, meaning that the critical angle was encountered at an offset h_c = 273 m (h_c = 2d *tan* θ_c). Considering the 150 m source-to-streamer layback present in this acquisition, pre-critical reflections will only be recorded for streamers three to eight. Beyond this point, energy will not be transmitted below

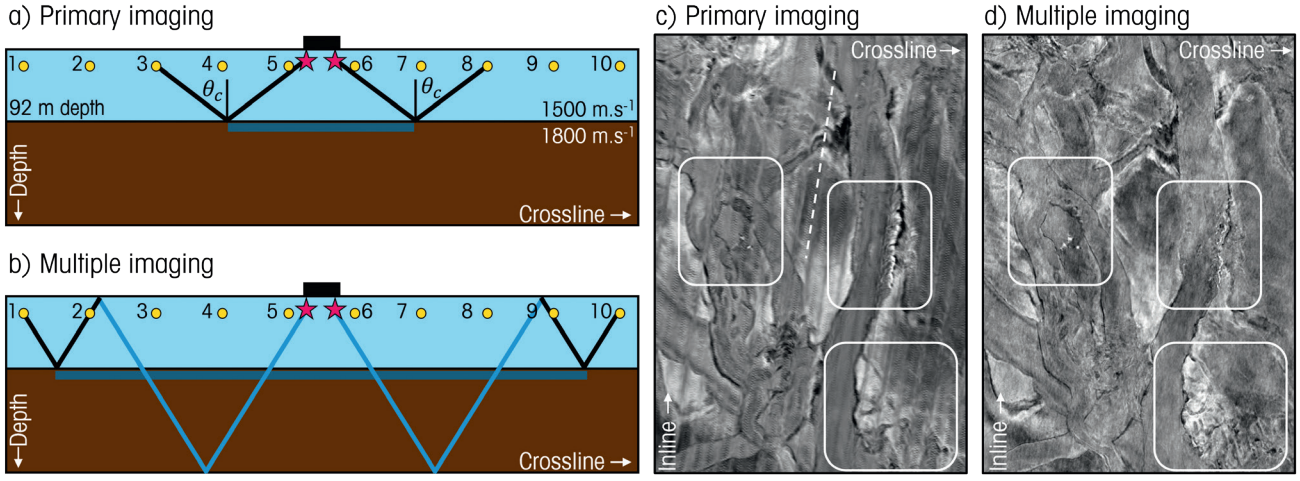

Figure 1 Ray diagrams relating to: a) Primary imaging, and b) Multiple imaging. Comparison of c) Primary imaging, and d) Multiple imaging for a 170 m depth slice from a towed-streamer acquisition in the Central North Sea.

[1] Viridien
* Corresponding author, E-mail: gordon.poole@viridiengroup.com
DOI: 10.3997/1365-2397.fb2024103

the water bottom, which will reduce deeper illumination. Wavelet stretch will also become a major issue beyond this point. Figure 1c shows a depth slice at 170 m from a common-shot primary wave-equation migration. Acquisition striping is observed along with low lateral resolution due to wavelet stretching. Figure 1d shows the same depth slice from multiple imaging. Injecting the data as secondary sources allows the imaging of receiver-side pegleg multiples (shown by the black ray-path in Figure 1b). This completed the illumination of the shallow section and revealed small-scale features as highlighted by the white boxes.

Multiple crosstalk

One pitfall of multiple imaging that has been discussed in the literature is multiple crosstalk (Poole et al., 2010, Lu et al., 2016). Multiple crosstalk relates to energy with the appearance of multiples contaminating the seismic image, caused by correlations of arrivals unrelated to one order of multiple separation. Causal crosstalk relates to contamination after an event; for example, a forward propagated primary correlating with a backward propagated second- or higher-order multiple. Anti-causal crosstalk relates to contamination above an event and may be caused, for example, by a forward propagated arrival correlating with a backward propagated primary.

Figure 2 discusses the formation of causal crosstalk using a simple synthetic consisting of a reflector at a 100 m depth within a constant-velocity subsurface of 1500 m.s^{-1}. Figure 2a introduces the ground-truth reflectivity and modelled data used for this analysis. These modelled data relate to a split-spread towed-streamer geometry including a primary arrival, P, first-order multiple, M_1, second-order multiple, M_2, and third-order multiple, M_3. In Figure 2b the modelled data has been propagated to a 100 m depth. The propagation used the one-way phase-shift-plus-interpolation (PSPI) strategy as outlined by Biondi (2006). A deconvolution imaging condition using the two gathers produced a strong response at the reflector due to the time alignment between P and M_1, M_1 and M_2, M_n and M_{n+1}, etc. The gathers were further propagated to image deeper, and at a 200 m depth, Figure 2c, the deconvolution imaging condition resulted in strong first-order crosstalk due to the time alignment between P and M_2, M_1 and M_3, M_n and M_{n+2}. The correlation between events more than one multiple order apart resulted in this non-physical event that was not present in the input model, Figure 2a. The phenomenon continued at a 300 m depth, Figure 2d, where each arrival correlated with an arrival three-orders later: M_n with M_{n+3}. Lu et al. (2016), describes a strategy to model the crosstalk, where the contamination may be subtracted in the image domain.

Our proposed causal crosstalk mitigation approach (Poole and Farshad, 2024) involved a cascaded least-squares multiple imaging scheme, where the residual left by a shallow least-squares multiple imaging result was used as the starting point for deeper least-squares multiple imaging. Figure 3a shows multiple imaging results from a towed-streamer dataset from the Norwegian North Sea. While the image is well focused in the shallow section, it is contaminated by water bottom multiple crosstalk (black arrow) and gas multiple crosstalk (white arrow). Shot gather input data is shown in Figure 3d and the residual after the least-squares multiple migration is shown in Figure 3e. The multiple migration has described most of the multiples in the input data, leaving the primary arrivals in the residual as expected. The least-squares cost function successfully described the multiples, but there was nothing in the scheme to prevent it doing so without causal crosstalk in the image. The proposed approach begins with least-squares multiple imaging of the water bottom, Figure 3b, produced using image-domain sparseness weights (Poole et al., 2021b). While a constant depth range is used for most migration algorithms, the image-domain sparseness weight volume used in this iterative least-squares technique masks image updates on each iteration to a discrete depth centred on the water bottom. The residual relating to this inversion, Figure 3f, was void of the water-bottom multiples observed on the input (Figures 3d and 3f, white arrows), but still contained longer-period multiples relating to the gas and deeper section (box on Figure 3f). The proposed approach continued by using this residual as input to imaging of the deeper section, Figure 3c. The image closely resembled the regular least-squares result (Figure 3a), but with less causal crosstalk from the water bottom. The corresponding residual is shown in Figure 3g, which looks similar to the regular

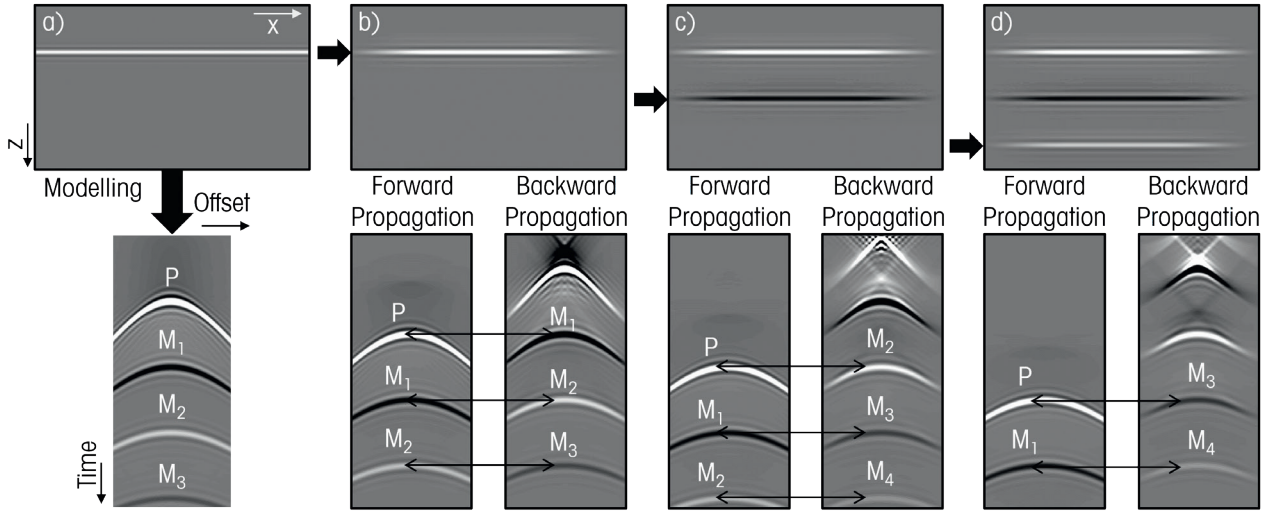

Figure 2 Synthetic analysis of causal crosstalk formation; a) Reflectivity input and modelled data, b) Image formation at 100 m depth, c) Image formation at 200 m depth, and d) Image formation at 300 m depth.

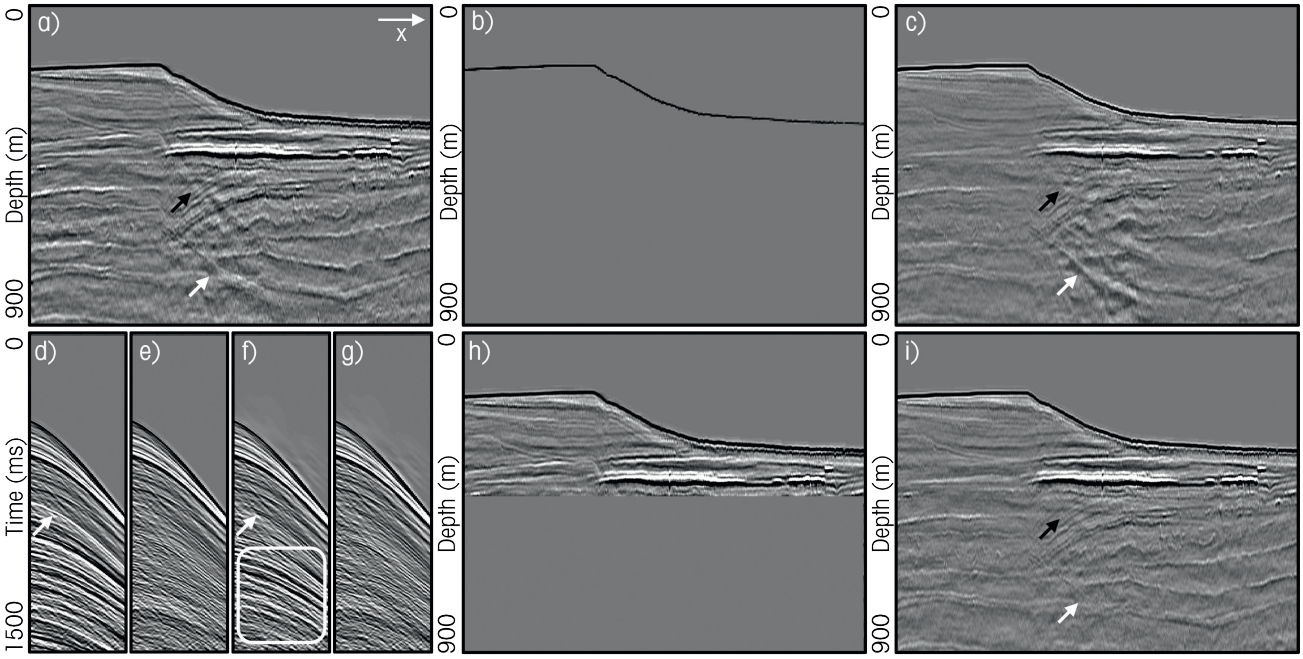

Figure 3 Illustration of cascaded least-squares multiple imaging: a) Regular least-squares multiple imaging, b) Constrained least-squares multiple imaging of the water bottom, c) Water bottom-driven cascaded multiple imaging, d) Shot gather starting residual, e) Shot gather residual after regular least-squares multiple imaging, f) Shot gather residual after constrained least-squares multiple imaging of the water bottom, g) Shot gather residual after water bottom driven cascaded multiple imaging, h) Constrained least-squares multiple imaging including water bottom and shallow gas, and i) Water bottom and gas-driven cascaded multiple imaging.

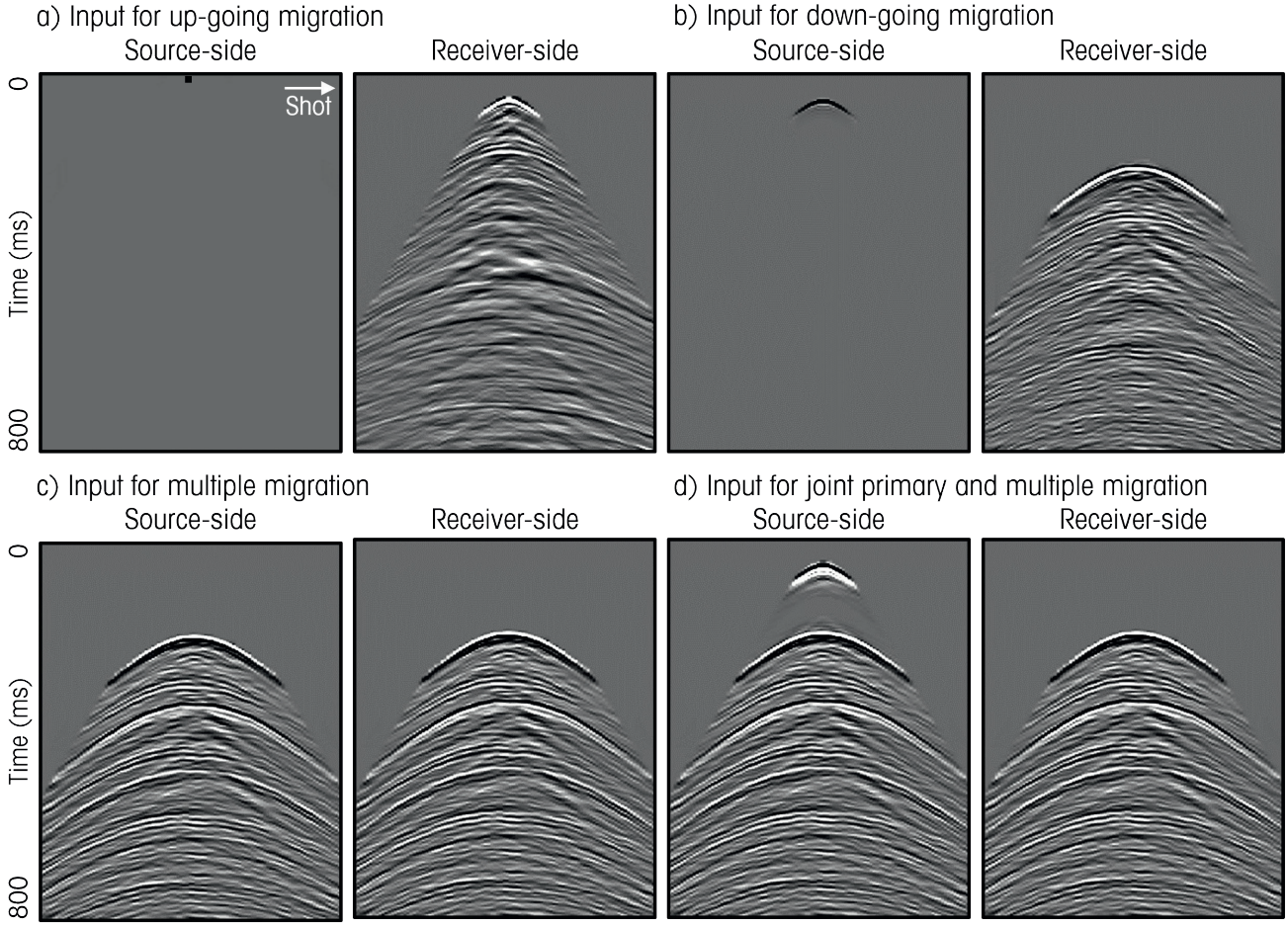

Figure 4 Input receiver gather data for the Utsira OBN dataset: a) Up-going migration, b) Down-going migration, c) Multiple migration, and d) Joint primary and multiple migration.

residual, Figure 3e. With this approach the algorithm is forced to describe water bottom multiples exclusively via the water bottom image, thus preventing deeper cross-talk contamination. Some gas-related multiple crosstalk was still present (Figure 3c white arrow) as the cascaded approach did not consider the gas multiple generators. For completeness, Figure 3h shows least-squares multiple imaging of the water bottom and gas arrivals, the residual from which was used to image the deeper section, Figure 3i. We now see that the causal crosstalk noise has been substantially reduced for both water bottom and gas-related multiple generators.

Subsurface illumination

Data used in the following discussion relates to an OBN acquisition in the Utsira area of the Norwegian North Sea. Shot carpet data with a 25 m × 50 m sampling were recorded by OBNs on a 50 m × 300 m grid. Based on well-known reciprocity principles, a source-side wavelet was injected at the node position and data after up-down deconvolution was input at the shot positions for the receiver-side backward propagation (Figure 4a). Figure 5a shows time slices at 236 ms and 370 ms (after stretching from depth to time) resulting from this up-going primary migration. The shallow image suffered from heavy acquisition striping owing to a lack of small reflection angles away from the receiver lines. This created significant uncertainty in the interpretation of the shallow section.

One well-known approach to improve shallow imaging involves the mirror migration of OBN down-going data (Grion et al., 2007). Mirror migration involves injecting and forward propagating a source wavelet at the mirror node location and using down-going data after demultiple at shot locations for the receiver-side backward propagation (Figure 4b); the resulting time slices are shown in Figure 5b. While the illumination is now relatively more continuous inbetween the receiver lines, the image is low fold, and some acquisition striping remains.

The migration of multiple reflections involves the injection of recorded data as secondary sources for both the source and receiver side (Figure 4c). The simultaneous illumination of all multiple orders occurs when forward propagated arrivals from the source side correlate with the following multiple order on the backward propagated wavefield from the receiver side. Compared to the down-going mirror migration, an increase in fold provides an improved signal-to-noise ratio (S/N), and illumination at smaller reflection angles has reduced wavelet stretching in the shallow section (Figure 5c). In addition, illumination beyond the receiver line layout is observed.

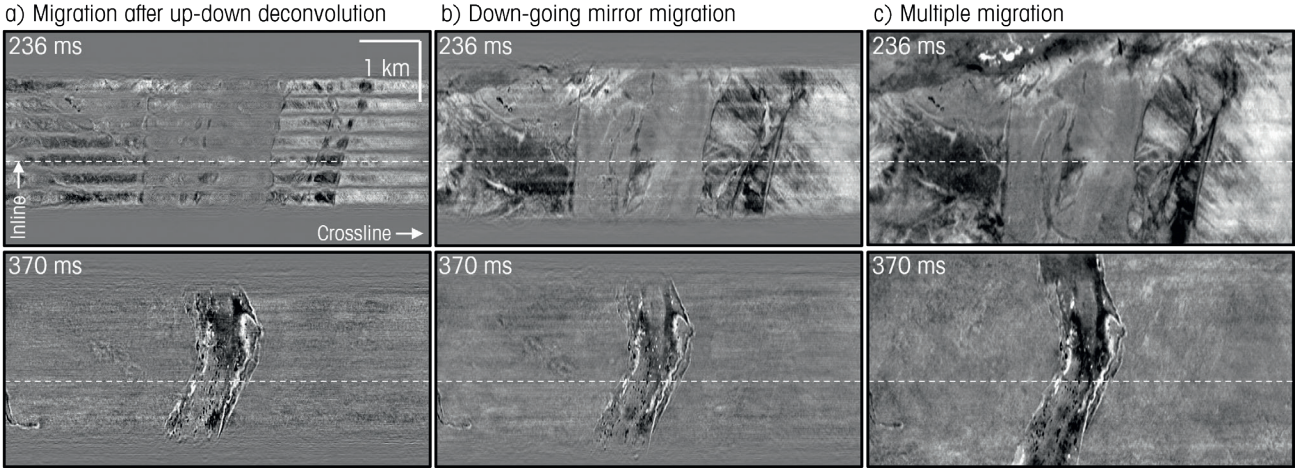

Figure 5 Imaging time slice results for the Utsira OBN dataset: a) Up-down deconvolution, b) Down-going mirror migration, and c) Multiple migration.

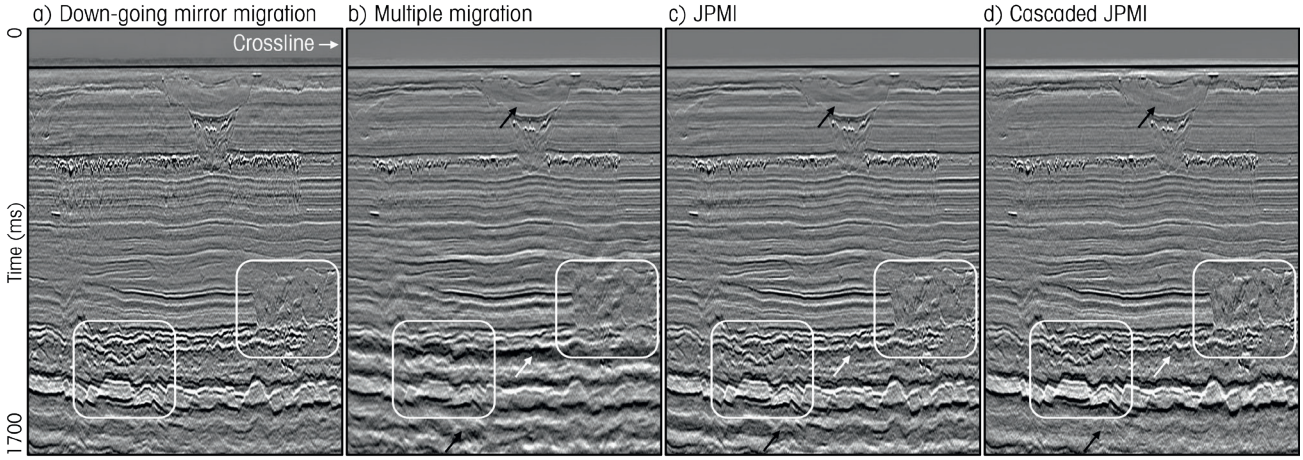

Figure 6 Imaging inline results for the Utsira OBN dataset: a) Down-going mirror migration, b) Multiple migration, c) Joint primary and multiple migration (JPMI), and d) Cascaded JPMI.

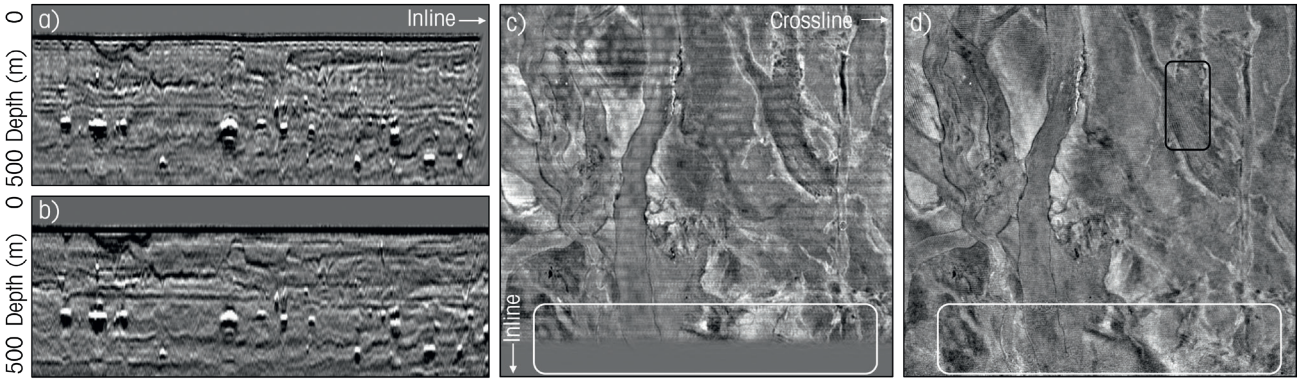

Figure 7 Imaging comparison from UK Central North Sea OBN dataset: a) Down-going mirror migration crossline, b) Down-going JPMI crossline, c) Down-going mirror migration depth slice, and d) JPMI depth slice.

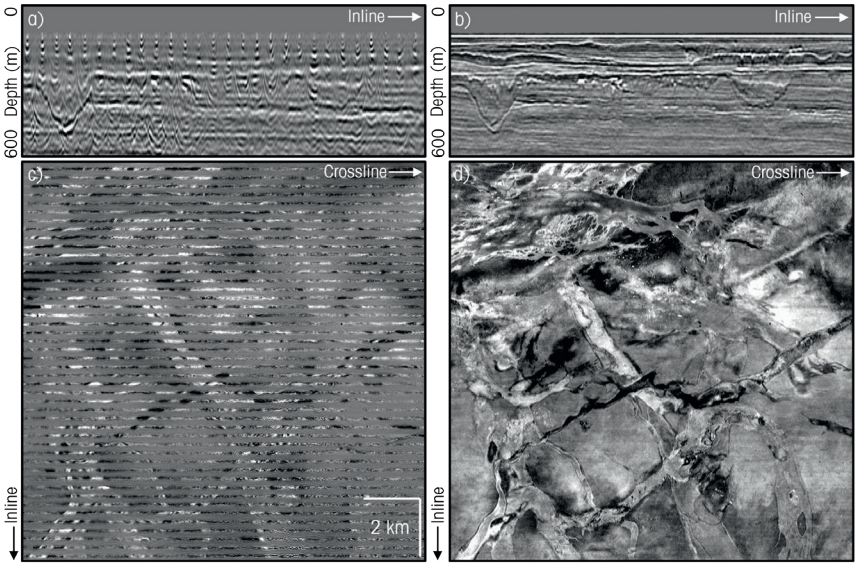

Figure 8 Imaging results from the Heimdal Terrace OBN dataset: a) Up-down deconvolution crossline, b) JPMI crossline, c) Up-down deconvolution depth slice, and d) JPMI depth slice. Depth slices are at 200 m.

In Figure 6a we show an inline (location annotated with dotted line on Figure 5) from the down-going mirror migration above one of the receiver lines. While the shallow section has been illuminated, it is contaminated by dipping noise due to being low-fold and suffers from some wavelet stretching. Figure 6b shows the same inline from multiple migration. While the image is sharp and coherent in the shallow, the S/N decreases as we go deeper, and crosstalk is prevalent throughout (see arrows). The S/N of multiple reflection contributions to the image is related to the number of orders of multiple that correlate for a given reflection. For short-period multiples, many multiple orders reverberate after each primary arrival resulting in a reliable and robust image. As the multiple period increases, the number of multiple orders in the input data decreases and the S/N decreases. Joint primary and multiple imaging (JPMI) may be achieved by including the direct arrival in the source-side data (Figure 4d). By doing so, we see that the S/N of the resulting image (Figure 6c) has increased, and anti-causal crosstalk contamination (white arrows) has been reduced as the primaries are largely described by the source-side direct arrival. Some causal crosstalk (black arrows), however, remains. Figure 6d shows the image after cascaded JPMI which has reduced causal crosstalk to negligible levels. Compared to the conventional down-going mirror migration route, the cascaded least-squares JPMI approach produced an image with comparable deep imaging and improved shallow imaging without the need for designature and demultiple preprocessing. Some residual noise remained in the shallow section as the least-squares nature of the solution partially modelled shallow noise that was present on the down-going mirror migration (Figure 6a).

Data examples

This OBN example comes from the UK Central North Sea, acquired with shots on a 50 m × 50 m grid. Figures 7a and 7b compare crossline sections perpendicular to the receiver lines for down-going mirror migration and JPMI, respectively. While the down-going mirror migration illuminates the shallow section, it is affected by receiver line striping. The JPMI image provides a similar level of lateral resolution with a reduction in striping in the shallow. Figures 7c and 7d show depth slices at 170 m for the area from the down-going mirror migration and JPMI, respectively. As well as providing a reduction in acquisition striping, we can see increased illumination at the bottom of the image (white rectangle), where imaging of multiples has provided imaging away from the receiver lines. Some slight residual shot-point acquisition footprint can be seen on the JPMI depth slice, e.g., black rectangle in Figure 7d.

The final example comes from the Heimdal Terrace OBN survey in the Norwegian North Sea acquired with a 25 m × 50 m shot sampling recorded by receivers on a 50 m × 300 m layout.

After up-down separation, these data were migrated to produce crossline and depth slice displays for a fast-track product, shown in Figures 8a and 8c respectively. The OBN line spacing has resulted in clear shallow striping making this shallow section unusable. The crossline and depth slice results from least-squares JPMI are shown in Figures 8b and 8d respectively. These JPMI results show a considerable improvement in shallow illumination and resolution, revealing shallow meandering channel systems and small-scale features throughout.

Conclusion

We have highlighted the limitations of shallow primary imaging and shown how the use of free-surface multiples may provide significant additional resolution in the shallow section. We have illustrated how the benefit of multiple imaging diminishes with increasing image depth and how multiple crosstalk may contaminate the multiple migration image. JPMI has been presented as a technique that can combine the illumination benefits of primaries and multiples while reducing anti-causal multiple crosstalk levels. Additionally, we have described a cascaded least-squares JPMI approach that is able to reduce causal multiple crosstalk to negligible levels. The use of multiples in imaging may provide potential for improved QC of shallow velocity models, allow the assessment of shallower targets, and potentially reduce the requirement for extensive site-survey acquisition in some areas.

Acknowledgements

We thank Viridien Earth Data for the towed-streamer data examples, data owners TGS and Axxis for the Utsira OBN images, Viridien Earth Data and TGS for the UK Central North Sea OBN data example, and Viridien Earth Data and TGS for the Heimdal Terrace OBN images. We also thank Viridien for its permission to publish this article.

References

Berkhout, A.J and Verschuur, D.J. [1994]. Multiple technology: Part 2, migration of multiple reflections. *64th Annual International Meeting, SEG*, Expanded Abstracts, 1497-1500.

Biondi, B.L. [2006]. 3D seismic imaging. *Investigations in Geophysics*, SEG publication.

Grion, S., Exley, R., Manin, M., Miao, X-G., Pica, A., Wang, Y., Granger, P-Y. and Ronan, S. [2007]. Mirror imaging of OBS data. *First Break*, **25**(11).

Lu, S., Whitmore, D., Valenciano, A., Chemingui, N. and Ronholt, G. [2016]. A practical crosstalk attenuation method for separated wavefield imaging. *86th Annual International Meeting*, *SEG*, Expanded Abstracts, 4235-4239.

Mujis, R., Holliger, K. and Robertsson, J.O.A. [2005]. Prestack depth migration of primary and surface-related multiple reflections. *75th Annual International Meeting, SEG*, Expanded Abstracts, 2107-2110.

Poole, G. [2021a]. Least-squares multiple imaging constrained jointly by OBN and towed-streamer data. *82nd EAGE Annual Conference & Exhibition*, Extended Abstracts.

Poole, G., Moore, H., Blaszczak, E., Kerrison, H., Keynejad, S., Taboga, A. and Chappell, M. [2021b]. Sparse wave-equation deconvolution imaging for improved shallow water demultiple. *82nd EAGE Annual Conference & Exhibition*, Extended Abstracts.

Poole, G. and Farshad, M. [2024]. Cascaded least-squares multiple imaging for reduced multiple crosstalk. *85th EAGE Annual Conference & Exhibition*, Extended Abstracts.

Poole, T.L., Curtis, A., Robertsson, J.O.A., and van Manen, D-J. [2010]. Deconvolution imaging conditions and cross-talk suppression. *Geophysics*, **75**(6), W1-W12.

Whitmore, N.D., Valenciano, A.A., Sollner, W. and Lu, S. [2010]. Imaging of primaries and multiples using a dual-sensor towed streamer. *80th Annual International Meeting, SEG*, Expanded Abstracts, 3187-3192.